Preparation of protein-loaded nanoparticles based on poly(succinimide)-oleylamine for sustained protein release: a two-step nanoprecipitation method

To cite this article: Xiangxun Chen *et al* 2024 *Nanotechnology* **35** 055101

OPEN ACCESS
IOP Publishing
Nanotechnology
Nanotechnology **35** (2024) 055101 (13pp)
https://doi.org/10.1088/1361-6528/ad0592

Preparation of protein-loaded nanoparticles based on poly(succinimide)-oleylamine for sustained protein release: a two-step nanoprecipitation method

Xiangxun Chen[1,2], **Shehzahdi S Moonshi**[1,2], **Nam-Trung Nguyen**[1,2] **and Hang Thu Ta**[1,2,*]

[1] School of Environment and Science, Griffith University, Brisbane, Queensland 4111, Australia
[2] Queensland Micro- and Nanotechnology Centre, Griffith University, Brisbane, Queensland 4111, Australia

E-mail: h.ta@griffith.edu.au

Received 29 August 2023
Accepted for publication 20 October 2023
Published 15 November 2023

Abstract

Currently, the treatment for acute disease encompasses the use of various biological drugs (BDs). However, the utilisation of BDs is limited due to their rapid clearance and non-specific accumulation in unwanted sites, resulting in a lack of therapeutic efficacy together with adverse effects. While nanoparticles are considered good candidates to resolve this problem, some available polymeric carriers for BDs were mainly designed for long-term sustained release. Thus, there is a need to explore new polymeric carriers for the acute disease phase that requires sustained release of BDs over a short period, for example for thrombolysis and infection. Poly(succinimide)-oleylamine (PSI-OA), a biocompatible polymer with a tuneable dissolution profile, represents a promising strategy for loading BDs for sustained release within a 48-h period. In this work, we developed a two-step nanoprecipitation method to load the model protein (e.g. bovine serum albumin and lipase) on PSI-OA. The characteristics of the nanoparticles were assessed based on various loading parameters, such as concentration, stirring rate, flow rate, volume ratio, dissolution and release of the protein. The optimised NPs displayed a size within 200 nm that is suitable for vasculature delivery to the target sites. These findings suggest that PSI-OA can be employed as a carrier for BDs for applications that require sustained release over a short period.

Keywords: sustained release, polysuccinimide, nanoprecipitation, biological drug loading, drug delivery

1. Introduction

Small-molecule drugs are primarily used for treatment of various diseases but are usually associated with unwanted off-target outcomes, resulting in adverse effects [1]. Biological drugs (BDs) are an increasingly popular class of drugs in treatment applications due to their more specific targeting effect [2], resulting in a market share that is estimated to be over 500 billion AUD by 2025 [3]. Nonetheless, this highly promising class of drugs is also limited by its intrinsic nature, which results in short plasma half-lives leading to wastage of administered dosage [4, 5]. Therefore, there is a need to resolve this problem.

Nanoparticles (NPs) have been widely employed as vehicles for effective delivery of BDs to target sites while

* Author to whom any correspondence should be addressed.

slowly releasing them over time for the desired therapeutic outcome [6–11]. Previously, several clinical trials have been conducted or completed on chemical drugs with nanodelivery that requires sustained release within a 48-h period, such as for pulmonary antibacterial and cardiovascular applications [12–17]. However, there is limited research on delivery of BDs using NPs as a carrier for release over a short period. Hence, there is the need to develop a strategy to provide localised delivery of BDs for sustained release within a 48-h period to maximise the utility of BDs.

Two of the most widely used types of NP for drug delivery are inorganic and liposomal NPs. However, inorganic NPs are more toxic and do not effectively load BDs [18]. Moreover, the instability of liposomal NPs and low encapsulation efficiency also lead to wastage of BDs. Polymeric NPs may therefore be a practical alternative. Polymeric NPs approved by the US Food and Drug Administration, such as polylactic-co-glycolic acid (PLGA) and polylactic acid (PLA), have been widely studied as vehicles for drug delivery [19]. However, the slow-release feature of PLGA and PLA (from days to a month) prevents them from being used for controlled drug release for acute disease applications such as thrombolysis and treatment of acute lung infections.

Here we employ polysuccinimide-oleylamine (PSI-OA) to prepare facile NPs to load BDs and allow sustained release of the BD over a 2-day period. PSI is non-toxic and non-mutagenic and has been utilised in various industrial and biomedical applications from sugar manufacturing to drug delivery systems [20–23]. Moreover, PSI can hydrolyse into poly(aspartic acid) under physiological conditions and is excreted from the body through renal and other physiological processes [24–29]. Oleylamine (OA) is a fatty acid that has been utilised for biomedical applications such as transdermal and anticancer treatment [30–32]. Previously, PSI-OA has been used to enhance the biocompatibility of a ^{19}F magnetic resonance imaging agent [33]. However, the use of PSI-OA in drug delivery remains unexplored. Thus, the present study will assess the efficacy of PSI-OA as a BD carrier for sustained release within 48 h.

A two-step nanoprecipitation method was developed to prepare BD-loaded PSI-OA NPs. This method avoids the requirement for elevated temperature, shear stress and ultrasound treatments that tend to denature BDs. A model protein, bovine serum albumin (BSA; 66 kDa), and model enzyme, lipase (~52 kDa), were used to mimic the loading of BDs. The current study optimises the conditions for BSA NPs and BSA loading and also assesses the basic characteristics such as size, polydispersity index, shape, zeta potential, loading efficiency, loading capacity, hydrolysis profile and release profile of the loaded NPs. The current study also assessed the activity of the BD after release from PSI-OA NPs.

2. Materials and methods

2.1. Chemicals

All non-listed chemicals were purchased from commercial suppliers at analytical grade. PSI-OA was synthesised in our lab using the existing protocol. BSA was obtained from Bovogen. Acetonitrile (ACN; lot 10913991) was purchased from LiChrosolv®. Aspartic acid, H_3PO_4 and sulfolane were purchased from Sigma. Dimethyl sulfoxide (DMSO; lot 1414511), dimethylformamide (DMF) and Pierce Micro-BCA™ Assay Kit (#23235) were purchased from Thermo Fisher.

2.2. Synthesis of PSI

PSI was synthesised using poly-condensation reactions of aspartic acid as described by Adelnia *et al* [34], Nakato *et al* [35] and Tomida *et al* [36]. Aspartic acid (21 g), H_3PO_4 (1.5 ml) and sulfolane (75 ml) were separately poured into a 100 ml three-necked flask immersed in a 185 °C oil bath under nitrogen gas flow with 150 rpm over-head stirring. After 6 h, the solution was precipitated in over ten times the volume of deionised water (dH_2O). The white PSI precipitate was washed three times with dH_2O under 4000*g* centrifugation for 10 min to remove excess solvent and chemicals and finally dried in a freeze drier or a vacuum oven to obtain white PSI powder. A 78% yield was achieved for PSI synthesis.

2.3. Synthesis of PSI-OA

To synthesise PSI-OA, typically 10 ml of 10% w/v PSI in DMF was mixed with 995 μl of OA and incubated under 500 rpm stirring using a stirring bar at 70 °C for 12 h. The final product was cooled at room temperature and washed three times with methanol using the same conditions as in section 2.2 to remove the redundant DMF. The final orange brown polymer powder was obtained from a freeze drier or vacuum oven.

2.4. Characterisation of NPs

The size, polydispersity index and zeta potential of the NPs were measured by dynamic light scattering with an Anton Paar Litesizer. The synthesised NPs were diluted ten times in either ACN or dH_2O before measurement. TEM images were taken on a JEOL-JEM-1010 TEM with an accelerating voltage of 80 kV. Protein concentration was evaluated using the micro-BCA protein assay according to the manufacturer's protocol.

2.5. Protein precipitation and loading

We modified the protocol of Morales-Cruz *et al* [37] and Nelemans *et al* [38]. BSA was first precipitated into small spherical NPs. Optimisation of this process encompassed various parameters whereby BSA at different concentrations was precipitated by dropwise addition of its non-solvent, ACN, at various flow rates and different BSA:ACN volume ratios under 500 rpm stirring using a magnetic stirring bar. The mixture was incubated for 5 min at room temperature under the same stirring condition. The intensity-weighted sizes and the polydispersity index (PDI) of the resultant BSA NPs (diluted 10 times in ACN) were measured by an Anton Paar Litesizer 500 (Graz, Austria).

We utilised the above BSA NP solution for the subsequent loading process. A volume of 1 ml of PSI-OA at 40 mg ml^{-1} was added to the BSA NP solution at different volume ratios. One millilitre of the mixed solution was transferred to different volume ratios of water in a beaker with different flow rates, with or without stirring. Details of concentrations, volume ratios and other details are listed in the results section. Data in this study are stated as mean ± standard deviation.

2.6. Loading efficiency and loading capacity

An indirect measurement method was used to calculate the loading efficiency (LE). WE centrifuged 1.5 ml of the NP solution at 16 100*g* for 15 min. The supernatant of the solution was collected to perform a micro-BCA assay. The amount of loaded protein for each group was calculated from the standard curve of the assay. The following equation was used to obtain the LE:

$$\text{LE}\,(\%) = \frac{\text{amount of proteinused} - \text{amount of supernatant protein}}{\text{amount of proteinused}} \times 100. \quad (1)$$

Loading capacity (LC) was calculated using the following equation:

$$\text{LC}\,(\%) = \frac{\text{amount of proteinused} - \text{amount of supernatant protein}}{\text{amount of polymerused} + \text{amount of proteinused}} \times 100. \quad (2)$$

2.7. In vitro release study

The NPs were washed twice, redispersed in phosphate-buffered saline (PBS) and incubated at 37 °C for 2 days. At different time points, 500 μl of the sample was taken and centrifuged at 16 100*g* for 15 min. The supernatant from the centrifuged sample was collected for measurement. A micro-BCA assay was performed to determine the BSA concentrations following the manufacturer's instructions. Data were used to construct a cumulative release profile graph.

2.8. Dissolution study

The NPs prepared in water were washed, redispersed in PBS, added to a 96-well plate and incubated at 37 °C to mimic physiological conditions [39–43]. The absorbance was measured over 48 h using a CLARIOstar® Plus plate reader (BMG Labtech) at 320 nm.

2.9. Viability study

The cytotoxicity was measured according to the company's manual using a PrestoBlue cell viability reagent with Chinese hamster ovary (CHO) cells. Briefly, CHO cells were seeded into 96-well plates at a density of 5000 cells per 100 μl solution per well and left overnight under 37 °C and 5% CO_2 for cell adherence. (The solution contained high-glucose Dulbecco's modified Eagle's medium, 10% heat-inactivated fetal bovine serum and 1% antibiotics.) Then the cells were incubated with 50, 100, 200, 400, 500 and 1000 ppm of the BSA-loaded PSI-OA NPs for 24 and 48 h. After the incubation treatment, the medium containing NPs was discarded and PrestoBlue reagent in PBS solution (one to ten dilution) added to each well. The plates were incubated under the same condition of cell adherence for 30 min after the addition of PrestoBlue. Finally, the plates were read in a CLARIOstar® Plus plate reader (BMG Labtech) to obtain the data.

2.10. Enzyme activity assay

Lipase activity was determined using *p*-nitrophenyl palmitate as the substrate. The protocol was modified from Margesin *et al* [44], Godoy *et al* [45] and Lam *et al* [46]. Typically, 100 μl of substrate solution consisted of 10 μl of 3 mg ml^{-1} *p*-nitrophenyl palmitate isopropanol solution, 89.6 μl of 50 mM Trix-HCl and 0.4 μl of Triton-X 100. The released NP PBS solution containing lipase was added to the substrate solution in a 1.5 ml Eppendorf tube and incubated at 37 °C for 60 min to start the reaction. The reaction was stopped by placing the tubes on ice for 10 min. The solution in the tubes was transferred to a 96-well plate and read in a CLARIOstar® Plus plate reader at 400 nm. The same process was performed for the freshly prepared lipase PBS solution to construct a standard curve as a control.

2.11. Statistical analysis

Data are presented as mean ± standard deviation. One-way analysis of variance (ANOVA) with a post-hoc Dunnet test were employed for significance testing, with a *p*-value $\leqslant$ 0.05 being considered statistically significant. Data analyses were performed using GraphPad Prism (GraphPad Software Inc.)

3. Results and discussion

3.1. BSA NP formation

Figure 1 summarises the synthesis procedure for the protein-loaded NPs. BSA NPs were produced by dropwise addition of

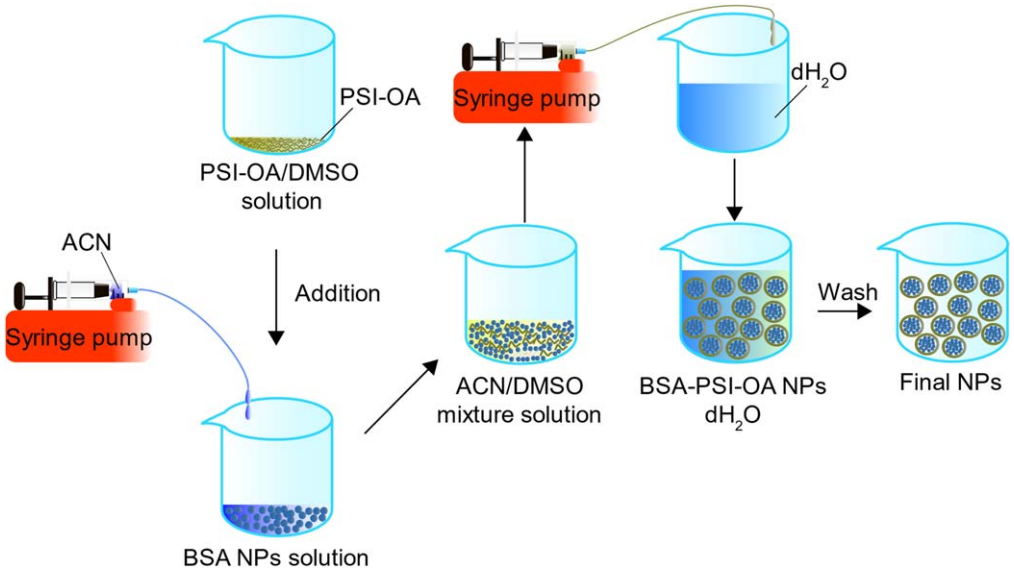

Figure 1. Scheme of the loading of BSA into PSI-OA via two-step nanoprecipitation.

ACN to BSA solution under stirring (figure 2(A)). Previous studies demonstrated the fewest protein aggregates with smaller particle sizes and uniform distribution when ACN was utilised as the non-solvent compared with acetone and ethanol [38]. Thus, ACN was selected as the non-solvent for BSA. To gain a more comprehensive understanding of protein precipitation, we assessed the parameters for preparing BSA NPs, such as the flow rate, BSA concentration and protein to non-solvent volume ratios.

Firstly, we assessed whether the increased flow rate of ACN to BSA solution affected the size of BSA NPs. Previous reports demonstrated that the flow rate of non-solvent had a significant effect on particle size [47]. The results of the current study confirmed this hypothesis. The increase in flow rates from 500 to 1200 μl min^{-1} resulted in a decrease in NP diameter and a decrease in PDI (improved NP uniformity) (figures 2(B) and (C)). The one-go group displayed a high standard deviation in the sizes and a significantly higher PDI compared with the 500, 800 and 1200 μl min^{-1} groups. Multiple peaks were observed in the size distribution of NPs from this group. Results demonstrate that using a syringe pump to control the flow rate to a higher level resulted in reproducible smaller-sized BSA NPs (94.2 $\pm$ 4.6 nm). The present study indicates that high flow rates are essential for future large-scale production, and the rate of 1200 μl min^{-1} was selected for the next optimisation steps in this study.

Secondly, the impact of BSA concentration on BSA NP size was assessed. The size of the samples increased with increasing BSA concentration (figure 2(E)). As the BSA concentration increased from 5 mg ml^{-1} to 10 mg ml^{-1} and 15 mg ml^{-1}, the particle size increased significantly from 53.2 $\pm$ 2.6 nm to 70.5 $\pm$ 2.3 nm and 90.1 $\pm$ 2.3 nm, respectively (figure 2(F)). However, PDI reduced from 18.4% to 14.5% and 13.8%, respectively, as the BSA concentration increased. The correlation between protein concentration and increase in NP size was consistent with previous studies [38, 48]. BSA NPs prepared with 5 mg ml^{-1} BSA solution had a larger PDI (20%) than the other groups. This may be explained by the LaMer concentration relationship model for precipitation whereby the solute concentration was not high enough to initiate precipitation [49], and thus resulted in non-uniform NP formation. Taken together, a BSA concentration of 10 mg ml^{-1} was selected for the rest of the study based on the size and PDI.

In the current study, an increase of ACN in the BSA to ACN volume ratio from 3.5 to 5.5 did not significantly affect the size distribution, size or PDI of the BSA NPs (figures 2(H)–(I)). Contrastingly, Tarhini *et al* [48] demonstrated that a decrease in non-solvent resulted in an increase in the diameters and size distributions of BSA NPs. However, other studies demonstrated a size reduction of zein protein NPs with increase in the non-solvent content [50]. It is suggested that the nature of the protein may contribute to this inconsistency.

Generally, the increase in non-solvent was thought to enhance the nucleation of the BSA NPs, whereby the rise in non-solvent content may cause a more rapid diffusion of solvent to non-solvent, thus reducing the diameter of the BSA NPs [51, 52]. While no significant difference was observed in the size and PDI of NPs with increased ACN in the BSA to ACN volume ratio in our study, a higher volume ratio was chosen for the loading step. The TEM image in figure 2(G) displays a spherical shape for the optimised BSA NPs prepared with 10 mg ml^{-1} BSA, a BSA:ACN volume ratio of 1:5.5 (e.g. 0.5 ml of 10 mg ml^{-1} BSA in dH_2O was added to 2.75 ml of ACN solution) and a flow rate of 1000 μl min^{-1} under 500 rpm stirring. The produced spherical NPs were stable without aggregation.

In this study, we did not investigate the effect of ACN solvent on the conformational changes and activity of BSA. However, existing literature supported the use of ACN to form BD particles with retained BD activity [37, 38, 53, 54]. In the future, when functional BDs are employed for disease

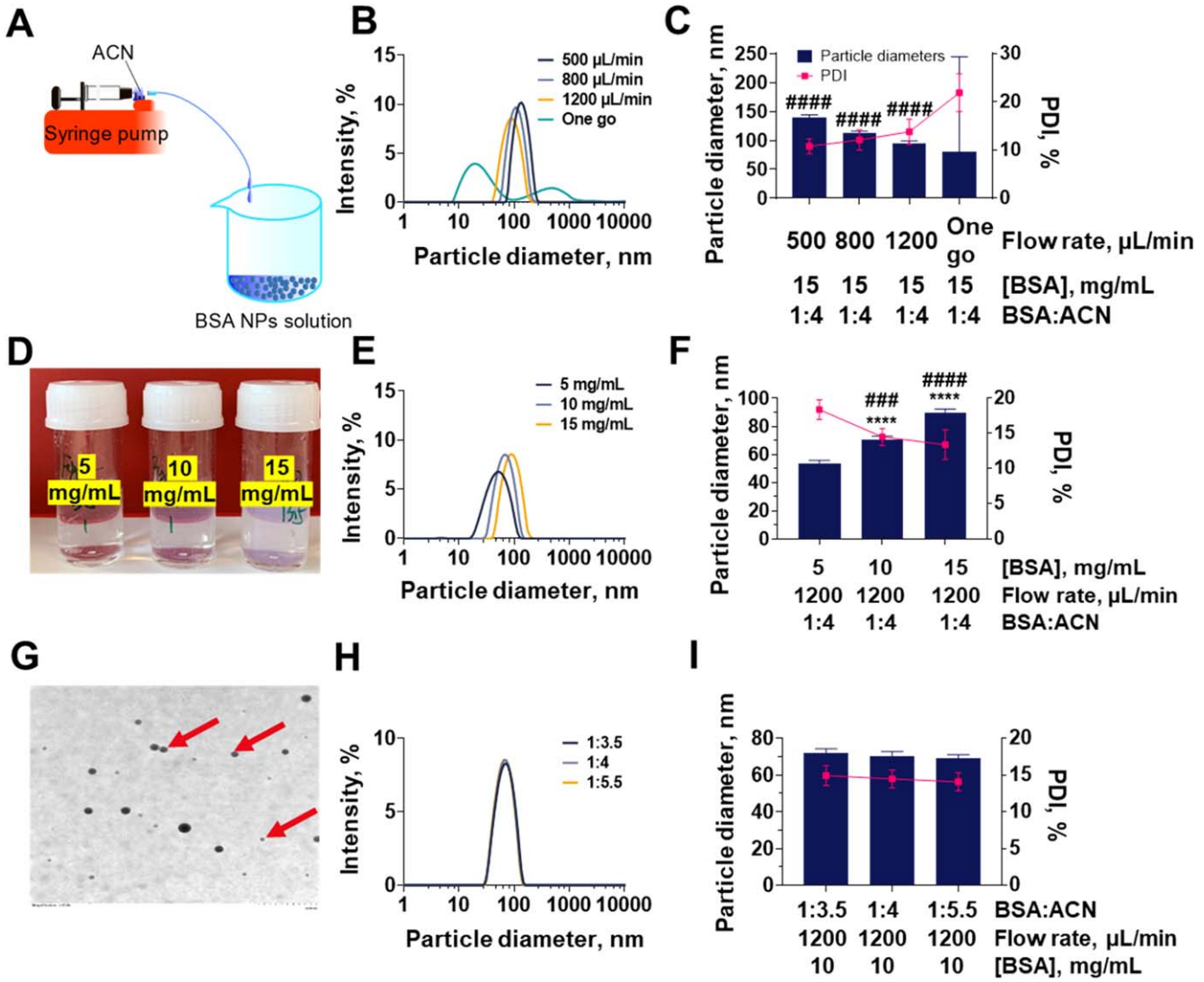

Figure 2. Optimisation of BSA NP synthesis. (A) Scheme of BSA NP production. (B), (C) Effect of flow rate upon addition of ACN to BSA solution on BSA NP size. (B) intensity-weighted distribution graph and (C) bar graph of the size and PDI of the BSA NPs synthesised using [BSA] = 15 mg ml^{-1} and BSA:ACN volume ratio = 1:4 with ACN flow rates of 500 μl min^{-1}, 800 μl min^{-1} and 1200 μl min^{-1} and by pipette in one go. ####, $p < 0.0001$ for PDIs compared with the one-go group. (D)–(F) Effect of BSA concentration on BSA NP size. (D) Appearance of the BSA NPs synthesised from different concentrations, from left to right 5 mg ml^{-1}, 10 mg ml^{-1} and 15 mg ml^{-1}. (E) Intensity-weighted distribution graph and (F) bar graph of the size and PDI of the BSA NPs synthesised using 5 mg ml^{-1}, 10 mg ml^{-1} and 15 mg ml^{-1} of BSA stock solution with a BSA:ACN volume ratio of 1:4 at an ACN flow rate of 1200 μl min^{-1}. ****, $p < 0.0001$ for the NP size compared with the 5 mg ml^{-1} group; ###, $p < 0.005$ for the PDIs compared with the 5 mg ml^{-1} group. (G)–(I) Effect of the BSA:ACN volume ratio on BSA NP size. (G) Representative TEM images of the BSA NPs synthesised with a BSA:ACN ratio of 1:5.5. (H) Intensity-weighted distribution graph and (I) bar graph of size and PDI of the BSA NPs synthesised using 10 mg ml^{-1} BSA stock solution with BSA:ACN volume ratios of 1:3.5, 1:4 and 1:5.5 at an ACN flow rate of 1200 μl min^{-1} and 500 rpm of stirring. $N = 3$ for all groups.

treatment we will thoroughly evaluate the impact of ACN on their activity.

3.2. Loading of BSA NPs in PSI-OA

We achieved protein loading by adding a mixture of BSA NP solution and PSI-OA solution into the non-solvent of the polymer, dH_2O (figure 3(A)). Parameters that affect the loading process include mixture:dH_2O volume ratio, PSI-OA:BSA NP volume ratio, flow rate of the addition of the mixture to water and stirring speed of the solution Firstly, the effect of the volume ratio of the mixture solution to dH_2O was investigated. Mixture:dH_2O volume ratios of 1:5, 1:9 and 1:12 were evaluated. Other parameters were kept constant.

Theoretically, a rise in non-solvent induces a higher supersaturation level, leading to a reduction in particle size [52, 55]. In our study, when the volume of dH_2O increased from five to nine parts (figure 3(C)), the size of the BSA-loaded NPs significantly decreased. However, increasing dH_2O to 12 parts did not reduce the NP size further but instead increased it. The particle size of the 1:9 group was significantly smaller than the 1:5 and 1:12 groups by about 26 nm (110 ± 7 nm versus 126 ± 3 nm and 126 ± 2 nm, respectively). In addition, PDI was not significantly different

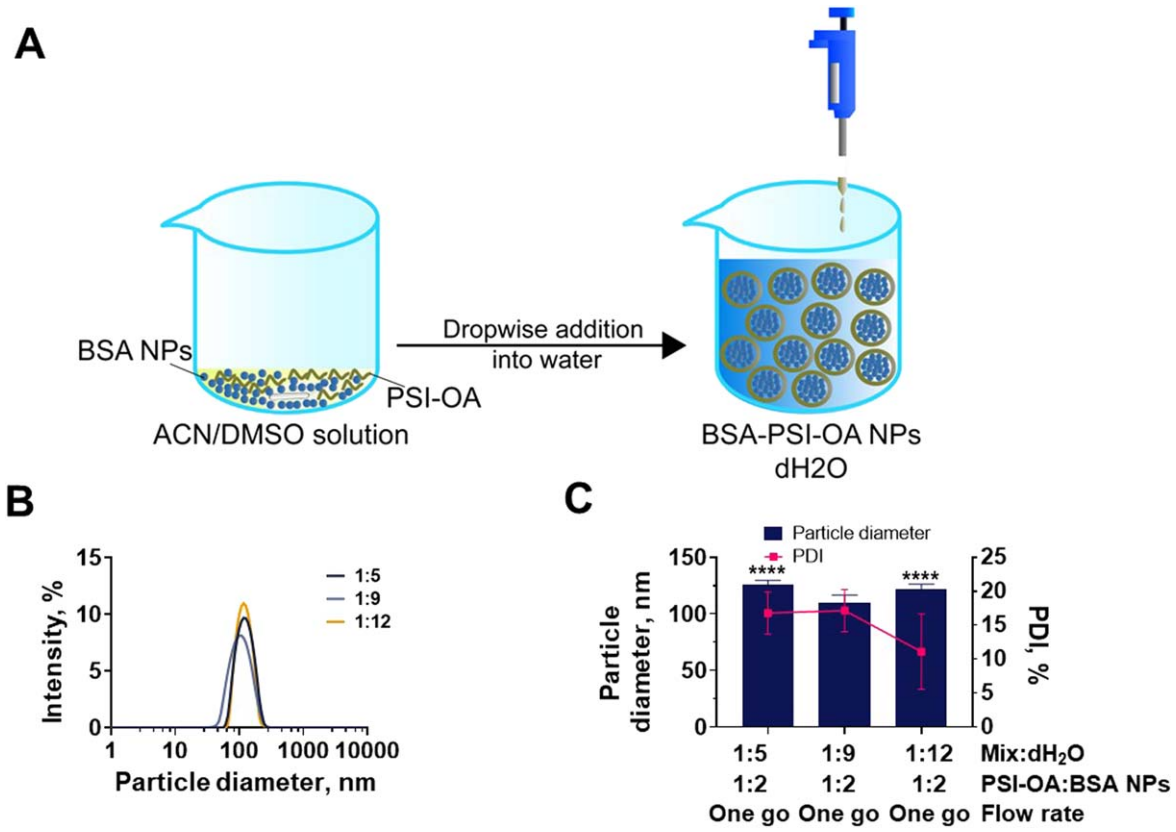

Figure 3. Optimisation of BSA-loaded PSI-OA NPs by varying the volume ratio of BSA NP/PSI-OA mixture and dH_2O. (A) Scheme of the production of BSA-loaded PSI-OA NPs. (B), (C) Effect of the volume ratio between PSI-OA/BSA NP mixture and water. (B) Intensity-weighted size distribution graph and (C) bar graph of size and PDI of the loaded NPs at different conditions. ****, $p < 0.0001$ for PDI compared with the 1:9 group. One part of 40 mg ml^{-1} PSI-OA/DMSO was added to two parts of the BSA precipitate. The mixed solution was then added to 5, 9 and 12 parts of dH_2O. One-way ANOVA with the Dunnet test. $N = 3$ for each group.

between the 1:5 and 1:9 groups (16.8% versus 17.2%, respectively). Nonetheless, the 1:12 group displayed a PDI of 11.1%, which was significantly lower than the 1:9 group. However, the PDI attained for the 1:9 group is still within an acceptable range (<20%) [56]. Whilst the hydrophobic nature of various polymers differs, this paper argues that the size variation of the loaded polymeric NPs in a supersaturated non-solvent solution requires a case-by-case analysis. Based on previously published studies, conflicting results have been reported whereby an increase in non-solvent effected an increase in size of polycaprolactone NPs, while a decrease in size was also observed in various other studies using polymers to load drugs [57–59]. At this stage, a smaller size of 110 nm and acceptable PDI is favourable for future delivery applications. Thus, we selected the ratio of PSI-OA and BSA NP mixture to water as 1:9.

The current study then assessed the impact of PSI-OA: BSA mixture ratios on the loaded NP size. One part of the polymer solution (40 mg ml^{-1}) was added to 2, 9 or 13 parts of BSA NPs to form a miscible mixture solution. The mixture solution was then added to nine parts of dH_2O to form the BSA-loaded NPs. Figures 4(A) and (B) show intensity-weighted particle sizes of 110 ± 7 nm, 81.1 ± 6.1 nm and 426 ± 1044 nm for 1:2, 1:6 and 1:13 groups, respectively. Notably, the standard deviation of the 1:13 group particle size was higher than for the other two groups. The increase of the BSA NP content made the size distribution wider. The 1:13 group formed unstable NPs that were not homogeneous, evidenced by the large standard deviation and PDI of the 1:13 group compared with the other two groups (PDI values of 17.2%, 21.7% and 24.9% for 1:2, 1:6 and 1:13 respectively; figure 4(B)). Even though the loading efficiency of the 1:13 group was significantly higher than for the 1:2 and 1:6 groups, the size at 426 ± 1044 nm and PDI over 20% were deemed unsuitable for drug delivery; the same applied to the 1:13 group (figure 4(B)). A large size would pose a risk of obstructing the pulmonary capillaries during circulation, subsequently causing adverse effects in human patients [60]. As the BSA NP content increased, the LE did not change significantly but the LC increased remarkably (figure 4(C)). Considering the size, PDI, LE and LC, a PSI-OA:BSA ratio of 1:2 was adopted for the rest of the study.

Next, the effect on NP size of the flow rate for the addition of PSI-OA/BSA NP mixture solution to dH_2O was assessed. The NP diameter of the fast pipetting one-go group was significantly lower than for the 100 μl min^{-1} and 1000 μl min^{-1} groups (110 ± 7 versus 127 ± 5 and 131 ± 4 nm, respectively; $p < 0.0001$ for both groups) (figures 4(D) and (E)). While the two-step nanoprecipitation method for loading BDs in the past did not examine the effect of addition rate in

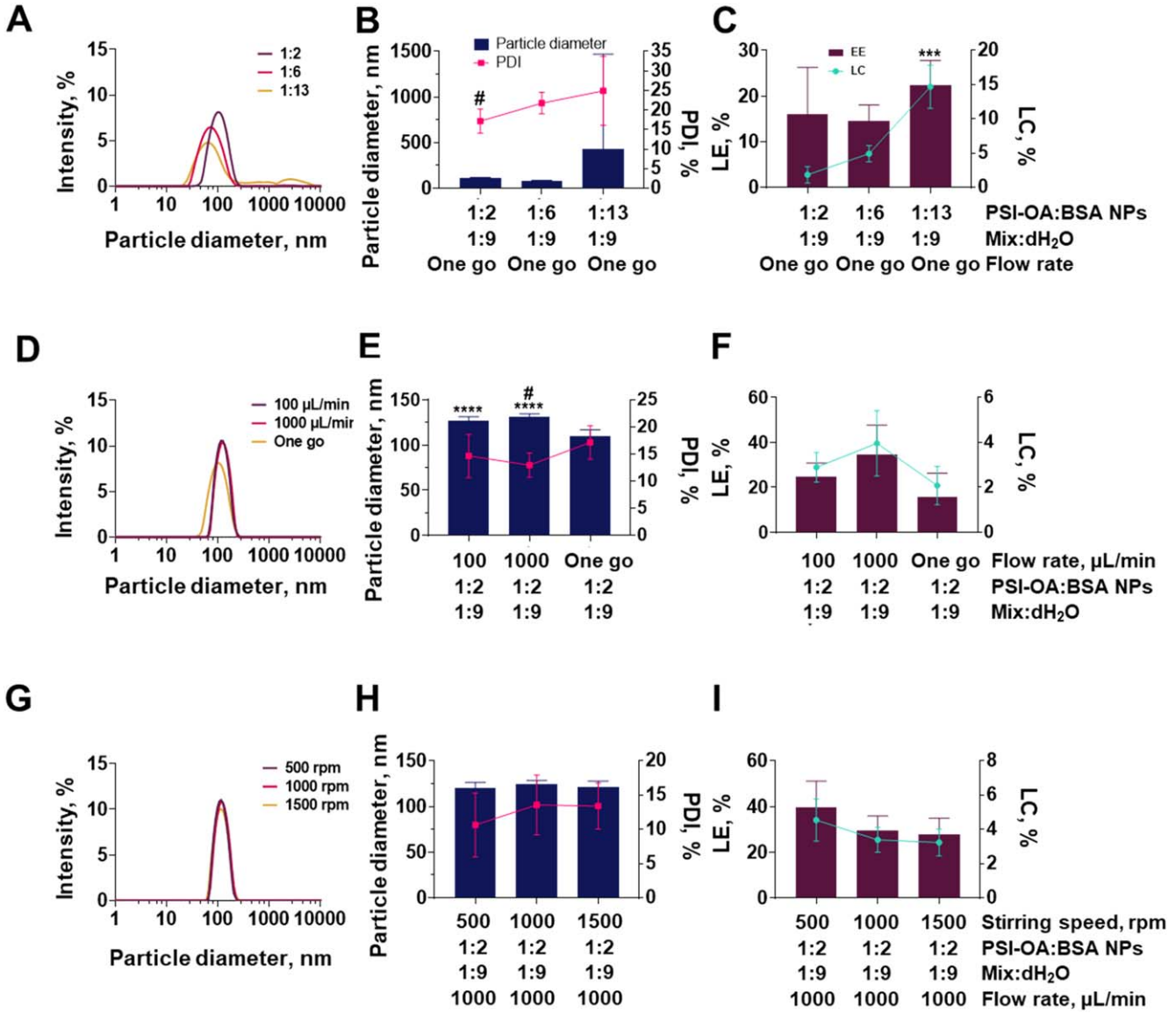

Figure 4. Optimisation of BSA-loaded PSI-OA NPs by varying PSI-OA:BSA NP volume ratios, flow rate of the mixture to water and stirring speed of the solution. (A)–(C) Effect of PSI-OA:BSA NP volume ratio. (A) intensity-weighted size distribution graph and (B) bar graph of size and polydispersity (PDI), #, PDI $p < 0.05$ for the 1:13 compared with the 1:2 group. (C) LE and LC of the loaded NPs at different PSI-OA to BSA volume ratios. ***, $p < 0.005$ for the LC of the 1:13 group compared with the 1:2 group. One part of 40 mg ml^{-1} PSI-OA/DMSO was added to 2, 6 and 13 parts of BSA NP solution. The mix solution was then added to nine parts of dH_2O for loading. (D)–(F) Effect of flow rate for adding a PSI-OA/BSA NP (1:9) mixture to dH_2O. (D) Intensity-weighted size distribution graph and (E) bar graph of size and PDI of the loaded NPs using different flow rates for a 1:9 mix to dH_2O volume ratio. ****, $p < 0.0001$ when comparing the sizes of 100 μl min^{-1} and 1000 μl min^{-1} groups with the one-go group. (F) LE and LC of the loaded NPs. (G)–(I) Effect of stirring rate at 500 rpm, 1000 rpm and 1500 rpm when adding a PSI-OA/BSA NP (1:9) mixture to water at 1000 μl min^{-1}. (G) Intensity-weighted size distribution graph. (H) Bar graph of size and PDI and (I) LE and LC of the loaded NPs. One-way ANOVA with a post-hoc Dunnet test. $N = 3$ for each group.

the final loading step, the increase in polymer flow rate in other modified nanoprecipitation methods using microfluidic devices and mixers for both BDs and non-BDs significantly reduced the particle size [61–63]. Even though the difference in PDI did not have statistical significance among the groups, the 1000 μl min^{-1} group had the lowest PDI of 13.0 $\pm$ 2.3%, and the other two groups had a slightly higher PDI than the 1 ml min^{-1} group (14.7 $\pm$ 4.0% and 17.2 $\pm$ 3.1% for 100 μl min^{-1} and the one-go group). Furthermore, the controlled flow rates increased the LE and LC of the particles, which is beneficial for future actual drug delivery. The LE of the one-go group (16.0 $\pm$ 10.3%) was lower than that of the 100 μl min^{-1} group and the 1000 μl min^{-1} group (24.9 $\pm$ 5.9% and 34.6 $\pm$ 13.1%, respectively). The LC followed the same trend (figure 4(F)). However, LE and LC amongst groups were not statistically significantly different. As a 1000 μl min^{-1} flow rate resulted in more homogeneous NPs with a slightly higher BSA loading this was therefore chosen as the optimised

Table 1. Optimised parameters for BSA-loaded PSI-OA NPs using nanoprecipitation.

Parameters	Value
Stirring speed	500 rpm
PSI-OA:BSA NPs	1:2
Mixture:dH_2O	1:9
Flow rate	1000 μl min^{-1}

parameter. The data suggested that the addition of the polymer/BSA NP mixture should be controlled and accelerated to achieve optimum BSA-loaded PSI-OA NPs.

Subsequently, we examined the effect of stirring speed on loaded NPs. Speeds of 500, 1000 and 1500 rpm were selected. The three stirring rate groups demonstrated no significant differences in particle diameter, including in PDI, LE and LC. The highest stirring rate (1500 rpm) only reduced the particle size by 1.4 nm when compared with the 500 rpm group (122 ± 6 nm versus 120 ± 6 nm; figures 4(G), (H)). A moderate speed of 1000 rpm produced particle sizes 4.6 nm larger than the 500 rpm group. Generally, increasing the stirring speed is considered beneficial for particle size reduction [64]. For example, Sanjeev *et al* [65] showed that a significant reduction in PLGA particle size could be achieved by increasing the stirring rate, but this was from 1000 rpm to 2500 rpm. In our study, we did not observe NP size reduction when increasing the stirring speed from 500 rpm to 1500 rpm.

Similarly, PDIs of NPs from all three groups were not significantly different. Although the 500 rpm group had a lower PDI than the 1000 rpm and 1500 rpm groups (10.7 ± 4.7%, 13.6 ± 3.4% and 13.4 ± 3.4%, respectively; figure 4(H)), the difference was not statistically significant. Besides, the 500 rpm group had a higher LE (39.9 ± 11.2% versus 29.5 ± 6.4% and 28.0 ± 6.9%, respectively) and LC (4.6 ± 1.2% versus 3.4 ± 0.7% and 3.2 ± 0.8%%, respectively) than the 1000 rpm and 1500 rpm groups. However, again, a statistically significant difference was not observed for LE and LC. These data suggested that stirring speed did not significantly affect the loaded NPs, but a lower speed resulted in a more favourable outcome. Previous studies showed that by increasing the agitation speed, the size of the particles decreases; however, after reaching a threshold the size increases as the speed increases further [66, 67]. In our study, the size increased slightly when the speed increased from 500 rpm to 1500 rpm, probably because this speed range was above the threshold. The further increase in stirring speed may also quicken the nanoprecipitation process of the polymer, and thus protein does not have enough time to be included within the NPs, resulting in a reduced loading efficiency. Therefore, a 500 rpm stirring speed in the loading step was chosen as the optimum speed in our study.

3.3. Dissolution and release study of the optimised NPs

In conclusion, table 1 summarises the optimal parameters for the synthesis of BSA-loaded PSI-OA NPs. The NPs prepared by the optimised protocol were homogeneous, displayed a spherical shape (figure 5(A)) with a size of 120 ± 6 nm, a PDI of 10.7 ± 4.7% and a zeta potential of −43.0 mV (figure 5(B)). NPs smaller than 200 nm are beneficial for biomedical applications such as intravenous drug delivery [68]. NPs in the range of approximately 150–200 nm have a longer circulation time than NPs smaller than 70 nm and larger than 300 nm in size [69]. In addition, NPs with a size of approximately 100 nm tend to circulate along the vascular wall [70, 71]. Hence, the NP with a size of ~120 nm developed in this study would have great potential for targeting vessel walls, for example thromboses which usually develop on the blood vessel wall.

The dissolution of the optimised BSA-loaded PSI-OA NPs and the release of BSA were investigated. Figure 5(C) shows that dissolution (hydrolysis) of the NPs in PBS at 37 °C was delayed for 3 h. After that, the NPs gradually dissolved and were completely hydrolysed after 36 h. Figure 5(D) establishes that 50% of BSA was released at approximately 16 h, 75% after 24 h and full release occurred after 40 h. These results demonstrate that PSI-OA can facilitate prolonged drug release under simulated human physiological conditions. These newly developed PSI-OA NPs offer sustained protein release and achieve complete release within 40 h, which is beneficial for acute biomedical applications requiring sustained release of BDs. In those applications, a sustained release of BDs over a short period could prevent the early breakdown of BDs by the body and avoid excessive aggregation in unwanted sites that could induce adverse effects, while ensuring the BD can be released quickly enough to the target sites, for example in emergency events such as heart attack and stroke.

3.4. In vitro cytoxicity study

The biocompatibility of the BSA-loaded PSI-OA NPs was assessed using the PrestoBlue cell viability reagent. CHO cells were incubated with a concentration range from 0.05 to 1 mg ml^{-1}. At 24 h, the cells maintained good viability (over 90%) at all NP concentrations (figure 5(E)). At 48 h, when all the BDs were released, the viability of the CHO cells was still at an acceptable level of over 80% (figure 5(F)). The highest PSI-OA concentration (1 mg ml^{-1}) resulted in cell viability of 95.1% and 97.4% at 24 and 48 h, respectively. These data support that the proposed NPs have good biocompatibility.

3.5. In vitro BD activity

To address whether simple nanoprecipitation can maintain the activity and size of various BDs with similar molecular weight, the optimised parameters with BSA were employed to load lipase. The lipase-loaded PSI-OA particles had a size of 85.1 ± 6.3 nm, a PDI of 19%, LE of 58.7 ± 1.5% and LC of 4.37 ± 0.1% (figures 6(A) and (E)). The intensity-distributed size of the lipase-loaded PSI-OA NPs was 35 nm lower than the BSA-loaded PSI-OA NPs. Moreover, the LE was 18.8% higher than BSA-loaded PSI-OA NPs, whereas LC was 0.3% lower than the BSA-loaded PSI-OA NPs. The release and dissolution behaviours of the lipase-loaded PSI-OA NPs were

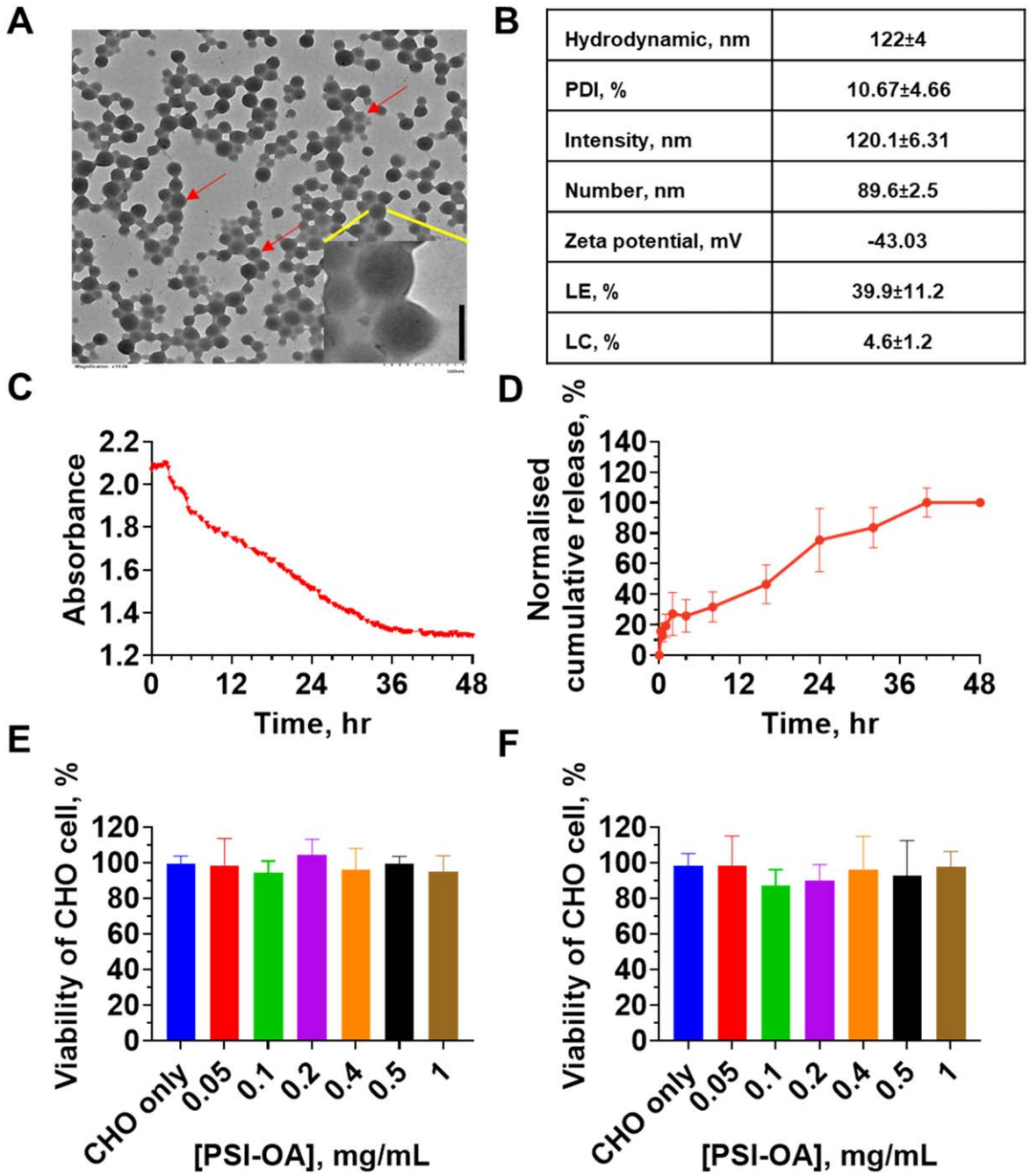

Figure 5. Characteristics of the optimised BSA-loaded PSI-OA NPs. (A) TEM images of the optimised BSA-loaded PSI-OA NPs (Vertical black scale bar: 100 nm), (B) Physical characteristics of the optimised BSA-loaded PSI-OA NPs, C) Dissolution profile of the NPs, (D) Normalised cumulative release profile of BSA from the NPs, and (E)–(F) Cytotoxicity study of BSA-loaded PSI-OA NPs after 24 and 48 h incubation (n = 3–5/group).

assessed in comparison with BSA. The dissolution of lipase-loaded PSI-OA NPs was slower than the BSA-loaded PSI-OA NPs, whereby the NPs started to disintegrate slowly for the first 15 h until full dissolution at 44–46 h (figure 6(B)). The release of the lipase corroborated the dissolution profile of NPs, whereby lipase was slowly released in the first 12 h at 17%, and 50% and 100% releases were attained at 35 h and 48 h, respectively. Whilst the release profiles of BSA and lipase were slightly different, 100% sustained release was acquired within 48 h.

To the best of our knowledge, this is also the first report on loading lipase in polymeric NPs. The activity of lipase released from the NPs was assessed to validate the use of PSI-OA to load BDs for drug delivery. Interestingly, the activity of the released lipase was retained compared with the freshly prepared control. The data presented in figure 6(D) suggested that the activity of the released lipase after dissolution for 48 h was maintained. This proof-of-concept data provide a good example for future studies to exploit PSI-OA for loading BDs while preserving BD activity.

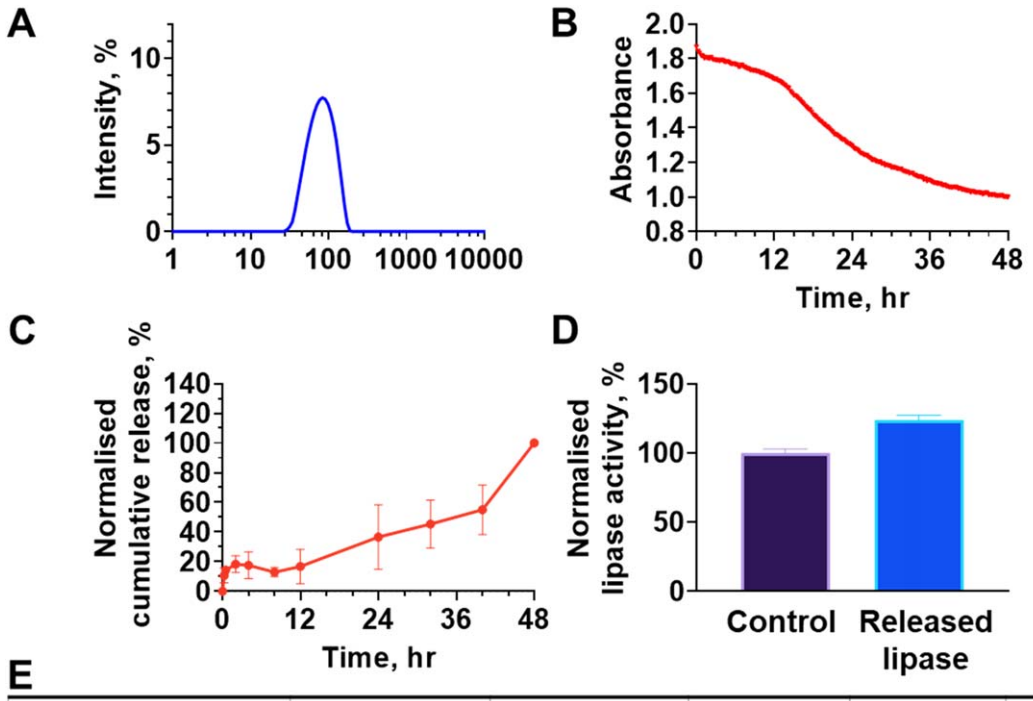

E

Hydrodynamic, nm	Intensity, nm	Number, nm	PDI, %	LE, %	LC %
80.0±5.2	85.1±6.3	47.0±5.0	19.0±1.7	58.7±1.5	4.37±0.1

Figure 6. Characteristics of the lipase-loaded PSI-OA NPs. (A) Intensity-weighted size distribution graph ($N = 3$). (B) Dissolution profile of the NPs. (C) Normalised cumulative release profile of lipase from the NPs. (D) Normalised lipase activity ($N = 4$ for control and $N = 6$ for released lipase group). (E) Physical characteristics of the lipase-loaded PSI-OA NPs ($N = 3$).

Furthermore, previously reported studies have employed nanoprecipitation method to load BDs such as lysozyme, α-chymotrypsin, amylase, trypsin inhibitor and catalase and their activity was retained [72]. However, these studies utilised various stabilisers such as polyvinyl acetate (PVA) during synthesis to avoid aggregation of the NPs and support NP formation during the nanoprecipitation process [38, 53, 54, 73, 74]. Residual PVA may potentially be cytotoxic and affect the release profile [75, 76]. Nonetheless, the incorporation of stabiliser may have an impact on BD bioavailability and retention time in the blood circulation [77]. In this study, we did not use stabiliser but were still able to obtain protein-loaded NPs with a small size (80–120 nm) and maintain activity. Previously, Morales-Cruz *et al* [37] used PLGA to load lysozyme (15 kDa) and α-chymotrypsin (25 kDa) and achieved a LC of 5%, accompanied by LEs of 94% and 74% for lysozyme and α-chymotrypsin respectively; however, the sizes of the NPs were larger than those synthesised in our current study (336 and 440 nm, respectively). These data demonstrate the advantage of PSI-OA NPs developed in our study for encapsulating BDs.

4. Conclusion and future perspectives

Nanoprecipitation is a method that can be employed to prepare NPs without surfactants or stabilisers, and would be an efficient method for encapsulating BDs. Nevertheless, only two articles have been published to date on using PLGA to load model proteins [37, 38]. In this study, we employed PSI-OA to load BDs for delivery. PSI has been used as the precursor for the synthesis of poly(aspartic acid) (PASP) by alkali hydrolysis. PSI could also be hydrolysed to PASP under milder condition (e.g. neutral pH) but at a much slower rate [78]. Due to these characteristics, PSI was employed for BD loading and release in this study. OA was grafted on the backbone of PSI to slow down the dissolution and hydrolysis of PSI NPs. The feasibility of this two-step nanoprecipitation method to load BSA with PSI-OA was evaluated in this study. Our data demonstrated that this polymer could achieve similar or even better results than previous studies using similar methods in the last decade [37, 38]. This is an essential move for PSI-OA towards drug delivery, especially for treatment of acute disease.

Using a two-step precipitation method, the present study has optimised the synthesis method using BSA as a model protein. This work reflects the utility and feasibility of using a two-step nanoprecipitation method for BD delivery, which is also transferable to different polymers. To the best of our knowledge, this work is the first to use PSI-OA to load BDs. The developed NPs could have a wide range of biomedical applications and have characteristics that are especially favourable for treatment of acute disease. For example, the NPs displayed a size of 120 nm and can travel along the blood vessel wall for various applications. In addition, the capability of the NPs to release BDs in a sustained manner within a short

time period is beneficial for acute treatment applications. The feasibility of PSI-OA to maintain the enzyme activity was also assessed. After *in vitro* release, the activity of the loaded lipase was retained. In future studies, BSA and lipase could be replaced by different BDs and binding ligands could be conjugated on the surface of the NPs for targeting purposes. Future research could also aim to maximise the use of PSI-OA to load more BDs for various applications.

Acknowledgments

This work is funded by National Health and Medical Research Council (HTT: APP1037310, APP1182347, APP2002827). XC is supported by a PhD scholarship from Griffith University. SSM is supported by a Griffith University fellowship. HTT is supported by a Heart Foundation Future Leader Fellowship (102761). The authors would like to acknowledge the Australian National Fabrication Facility (Queensland Node) access to key items of equipment.

Data availability statement

All data that support the findings of this study are included within the article (and any supplementary files).

Conflicts of interest

There is no conflict to report.

ORCID iDs

Xiangxun Chen https://orcid.org/0000-0002-2208-1038
Shehzahdi S Moonshi https://orcid.org/0000-0003-2048-595X
Nam-Trung Nguyen https://orcid.org/0000-0003-3626-5361
Hang Thu Ta https://orcid.org/0000-0003-1188-0472

References

[1] Rao M S, Gupta R, Liguori M J, Hu M, Huang X, Mantena S R, Mittelstadt S W, Blomme E A G and Van Vleet T R 2019 Novel computational approach to predict off-target interactions for small molecules *Frontiers Big Data* **2** 1–17
[2] Makurvet F D 2021 Biologics vs. small molecules: drug costs and patient access *Med. Drug Discovery* **9** 100075
[3] PRNewswire 2022 https://prnewswire.com/news-releases/global-biologics-market-analysis-report-2022-2025-−2030-featuring-merck–co-abbvie-f-hoffmann-la-roche-johnson–johnson–pfizer-301530433.html, Accessed 02.11 2023
[4] Modi N B, Eppler S, Breed J, Cannon C P, Braunwald E and Love T W 1998 Pharmacokinetics of a slower clearing tissue plasminogen activator variant, TNK-tPA, in patients with acute myocardial infarction *Thromb. Haemost.* **79** 134–9
[5] Skalko-Basnet N 2014 Biologics: the role of delivery systems in improved therapy *Biologics* **8** 107–14
[6] De Jong W H and Borm P J 2008 Drug delivery and nanoparticles:applications and hazards *Int. J. Nanomed.* **3** 133–49
[7] Ta H T, Dass C R, Larson I, Choong P F and Dunstan D E 2009 A chitosan hydrogel delivery system for osteosarcoma gene therapy with pigment epithelium-derived factor combined with chemotherapy *Biomaterials* **30** 4815–23
[8] Banun V J *et al* 2023 Protein nanoparticles for enhanced oral delivery of coenzyme-Q10: *in vitro* and in silico studies *ACS Biomater. Sci. Eng.* **9** 2846–56
[9] Perera B, Wu Y, Nguyen N T and Ta H T 2023 Advances in drug delivery to atherosclerosis: Investigating the efficiency of different nanomaterials employed for different type of drugs *Mater. Today Bio.* **22** 100767
[10] Arndt N, Tran H D N, Zhang R, Xu Z P and Ta H T 2020 Different approaches to develop nanosensors for diagnosis of diseases *Adv. Sci. (Weinh.)* **7** 2001476
[11] Pickett J R, Wu Y, Zacchi L F and Ta H T 2023 Targeting endothelial VCAM-1 in atherosclerosis: drug discovery and development of VCAM-1-directed novel therapeutics *Cardiovasc. Res.* **119** 2278–93
[12] Siegel S, Clock J A, Hoeft J, Chan B, Sullivan P E, Philley J, Strnad L C, Griffith D E and Winthrop K L 2018 Open-label trial of amikacin liposome inhalation suspension in *M. abscessus* lung disease *A58. Non-Tuberculous Mycobacteria: Off The Beaten Track American Thoracic Society 2018 International Conference* (American Thoracic Society 2018) A7669–7669
[13] Olivier K N, Griffith D E, Eagle G, McGinnis J P, Micioni L, Liu K, Daley C L, Winthrop K L, Ruoss S and Addrizzo-Harris D J 2017 Randomized trial of liposomal amikacin for inhalation in nontuberculous mycobacterial lung disease *Am. J. Resp. Crit. Care. Med.* **195** 814–23
[14] Bilton D *et al* 2020 Amikacin liposome inhalation suspension for chronic *Pseudomonas aeruginosa* infection in cystic fibrosis *J. Cyst. Fibros.* **19** 284–91
[15] Velino C, Carella F, Adamiano A, Sanguinetti M, Vitali A, Catalucci D, Bugli F and Iafisco M 2019 Nanomedicine approaches for the pulmonary treatment of cystic fibrosis *Front. Bioeng. Biotechnol.* **7** 406
[16] Jia B *et al* 2022 Comparison of drug-eluting stent with bare-metal stent in patients with symptomatic high-grade intracranial atherosclerotic stenosis: a randomized clinical trial *JAMA Neurol.* **79** 176–84
[17] Chalmers J D, Cipolla D, Thompson B, Davis A M, Donnell A, Tino G, Gonda I, Haworth C and Froehlich J 2020 Changes in respiratory symptoms during 48-week treatment with ARD-3150 (inhaled liposomal ciprofloxacin) in bronchiectasis: results from the ORBIT-3 and −4 studies *Eur. Resp. J.* **56** 2000110
[18] De Matteis V 2017 Exposure to inorganic nanoparticles: routes of entry, immune response, biodistribution and *in vitro*/*in vivo* toxicity evaluation *Toxics* **5** 1–21
[19] Elmowafy E M, Tiboni M and Soliman M E 2019 Biocompatibility, biodegradation and biomedical applications of poly(lactic acid)/poly(lactic-co-glycolic acid) micro and nanoparticles *J. Pharmaceut. Invest.* **49** 347–80
[20] Tudorachi N and Chiriac A P 2011 TGA/FTIR/MS study on thermal decomposition of poly (succinimide) and sodium poly (aspartate) *Polym. Test.* **30** 397–407
[21] Mazo G Y, Mazo J, Vallino B and Ross R J 1999 Production of polysuccinimide and polyaspartate in thioether solvents *US Patent* US5939522A
[22] Chen H, Xu W, Chen T, Yang W, Hu J and Wang C 2005 Aggregation of biodegradable amphiphilic poly (succinimide-co-N-propyl aspartamide) and poly(N-dodecyl

aspartamide-co-N-propyl aspartamide) in aqueous medium and its preliminary drug-released properties *Polymer* **46** 1821–7
[23] Yeh J-C, Hsu Y-T, Su C-M, Wang M-C, Lee T-H and Lou S-L 2014 Preparation and characterization of biocompatible and thermoresponsive micelles based on poly(N-isopropylacrylamide-co-N,N-dimethylacrylamide) grafted on polysuccinimide for drug delivery *J. Biomater. Appl.* **29** 442–53
[24] Huang S, Bai M and Wang L 2013 General and facile surface functionalization of hydrophobic nanocrystals with poly (amino acid) for cell luminescence imaging *Sci. Rep.* **3** 2023
[25] Juriga D, Laszlo I, Ludanyi K, Klebovich I, Chae C H and Zrinyi M 2018 Kinetics of dopamine release from poly (aspartamide)-based prodrugs *Acta Biomater.* **76** 225–38
[26] Adelnia H, Sirous F, Blakey I and Ta H T 2023 Metal ion chelation of poly (aspartic acid): From scale inhibition to therapeutic potentials *Int. J. Biol. Macromol.* **229** 974–93
[27] Adelnia H, Tran H D N, Little P J, Blakey I and Ta H T 2021 Poly(aspartic acid) in biomedical applications: from polymerization, modification, properties, degradation, and biocompatibility to applications *ACS Biomater. Sci. Eng.* **7** 2083–105
[28] Adelnia H, Blakey I, Little P J and Ta H T 2019 Hydrogels based on poly(aspartic acid): synthesis and applications *Front. Chem.* **7** 755
[29] Adelnia H, Moonshi S S, Wu Y, Bulmer A C, Mckinnon R, Fastier-Wooller J W, Blakey I and Ta H T 2023 A bioactive polymer nanoparticle for synergistic vascular anti-calcification *ACS Nano* **17** 18775–91
[30] Liu Z, Chen X, Huang Z, Shi J, Liu C, Cao S, Yan H and Lin Q 2021 Self-assembled oleylamine grafted alginate aggregates for hydrophobic drugs loading and controlled release *Int J Polym Mater. Polym. Biomater.* **72** 212–23
[31] Hsiao P F, Peng S, Tang T C, Lin S Y and Tsai H C 2016 Enhancing the *in vivo* transdermal delivery of gold nanoparticles using poly(ethylene glycol) and its oleylamine conjugate *Int. J. Nanomed.* **11** 1867–78
[32] Sun H *et al* 2012 Influences of surface coatings and components of FePt nanoparticles on the suppression of glioma cell proliferation *Int. J. Nanomed.* **7** 3295–307
[33] Guo C, Xu S, Arshad A and Wang L 2018 A pH-responsive nanoprobe for turn-on 19F-magnetic resonance imaging *Chem. Commun.* **54** 9853–6
[34] Adelnia H, Blakey I, Little P J and Ta H T 2023 Poly (succinimide) nanoparticles as reservoirs for spontaneous and sustained synthesis of poly(aspartic acid) under physiological conditions: potential for vascular calcification therapy and oral drug delivery *J. Mater. Chem.* B **11** 2650–62
[35] Nakato T, Kusuno A and Kakuchi T 2000 Synthesis of poly (succinimide) by bulk polycondensation of L-aspartic acid with an acid catalyst *J. Polym. Sci.*A **38** 117–22
[36] Tomida M, Nakato T, Matsunami S and Kakuchi T 1997 Convenient synthesis of high molecular weight poly (succinimide) by acid-catalysed polycondensation of l-aspartic acid *Polymer* **38** 4733–6
[37] Morales-Cruz M, Flores-Fernández G M, Morales-Cruz M, Orellano E A, Rodriguez-Martinez J A, Ruiz M and Griebenow K 2012 Two-step nanoprecipitation for the production of protein-loaded PLGA nanospheres *Results Pharma. Sci.* **2** 79–85
[38] Nelemans L C, Buzgo M and Simaite A 2021 Optimization of protein precipitation for high-loading drug delivery systems for immunotherapeutics *Proceedings* **78** 2–9
[39] Benhabbour S R *et al* 2019 Ultra-long-acting tunable biodegradable and removable controlled release implants for drug delivery *Nat. Commun.* **10** 4324
[40] Bossion A, Zhu C, Guerassimoff L, Mougin J and Nicolas J 2022 Vinyl copolymers with faster hydrolytic degradation than aliphatic polyesters and tunable upper critical solution temperatures *Nat. Commun.* **13** 2873
[41] D'Amato A R, Puhl D L, Ellman S A T, Balouch B, Gilbert R J and Palermo E F 2019 Vastly extended drug release from poly(pro-17β-estradiol) materials facilitates *in vitro* neurotrophism and neuroprotection *Nat. Commun.* **10** 4830
[42] Sarmadi M *et al* 2022 Experimental and computational understanding of pulsatile release mechanism from biodegradable core–shell microparticles *Sci. Adv.* **8** eabn5315
[43] Kolishetti N, Dhar S, Valencia P M, Lin L Q, Karnik R, Lippard S J, Langer R and Farokhzad O C 2010 Engineering of self-assembled nanoparticle platform for precisely controlled combination drug therapy *Proc. Natl Acad. Sci. USA* **107** 17939–44
[44] Margesin R, Feller G, Hämmerle M, Stegner U and Schinner F 2002 A colorimetric method for the determination of lipase activity in soil *Biotechnol. Lett.* **24** 27–33
[45] Godoy P, Mourenza Á, Hernández-Romero S, González-López J and Manzanera M 2018 Microbial production of ethanol from sludge derived from an urban wastewater treatment plant *Front. Microbiol.* **9** 2634
[46] Lam L and Ilies M A 2022 Evaluation of the impact of esterases and lipases from the circulatory system against substrates of different lipophilicity *Int. J. Mol. Sci.* **23** 1–14
[47] Ali H S M, Blagden N, York P, Amani A and Brook T 2009 Artificial neural networks modelling the prednisolone nanoprecipitation in microfluidic reactors *Eur. J. Pharm. Sci.* **37** 514–22
[48] Tarhini M, Benlyamani I, Hamdani S, Agusti G, Fessi H, Greige-Gerges H, Bentaher A and Elaissari A 2018 Protein-based nanoparticle preparation via nanoprecipitation method *Materials (Basel)* **11** 1–18
[49] LaMer V K and Dinegar R H 1950 Theory, production and mechanism of formation of monodispersed hydrosols *J. Am. Chem. Soc.* **72** 4847–54
[50] Li F *et al* 2017 Size-controlled fabrication of zein nano/microparticles by modified anti-solvent precipitation with/without sodium caseinate *Int. J. Nanomed.* **12** 8197–209
[51] Wang G, Siggers K, Zhang S, Jiang H, Xu Z, Zernicke R F, Matyas J and Uludağ H 2008 Preparation of BMP-2 containing bovine serum albumin (BSA) nanoparticles stabilized by polymer coating *Pharm. Res.* **25** 2896–909
[52] Tao J, Chow S F and Zheng Y 2019 Application of flash nanoprecipitation to fabricate poorly water-soluble drug nanoparticles *Acta Pharm. Sin.*B **9** 4–18
[53] De Queiroz J L C, De Araújo Costa R O, Rodrigues Matias L L, De Medeiros A F, Teixeira Gomes A F, Santos Pais T D, Passos T S, Maciel B L L, Dos Santos E A and De Araújo Morais A H 2018 Chitosan-whey protein nanoparticles improve encapsulation efficiency and stability of a trypsin inhibitor isolated from tamarindus indica L *Food Hydrocolloids* **84** 247–56
[54] Liao R, Pon J, Chungyoun M and Nance E 2020 Enzymatic protection and biocompatibility screening of enzyme-loaded polymeric nanoparticles for neurotherapeutic applications *Biomaterials* **257** 120238
[55] Martínez Rivas C J, Tarhini M, Badri W, Miladi K, Greige-Gerges H, Nazari Q A, Galindo Rodríguez S A, Román R, Fessi H and Elaissari A 2017 Nanoprecipitation process: from encapsulation to drug delivery *Int. J. Pharm.* **532** 66–81
[56] Danaei M, Dehghankhold M, Ataei S, Hasanzadeh Davarani F, Javanmard R, Dokhani A, Khorasani S and Mozafari M 2018 Impact of particle size and polydispersity index on the

clinical applications of lipidic nanocarrier systems *Pharmaceutics* **10** 57
[57] Limayem Blouza I, Charcosset C, Sfar S and Fessi H 2006 Preparation and characterization of spironolactone-loaded nanocapsules for paediatric use *Int. J. Pharm.* **325** 124–31
[58] Kakran M, Sahoo N G, Tan I-L and Li L 2012 Preparation of nanoparticles of poorly water-soluble antioxidant curcumin by antisolvent precipitation methods *J. Nanopart. Res.* **14** 1–11
[59] Khan S A and Schneider M 2013 Improvement of nanoprecipitation technique for preparation of gelatin nanoparticles and potential macromolecular drug loading *Macromol. Biosci.* **13** 455–63
[60] Tees D F J, Sundd P and Goetz D J 2006 A flow chamber for capillary networks: leukocyte adhesion in capillary-sized, ligand-coated micropipettes *Principles of Cellular Engineering* ed M R King (Burlington, MA: Academic) 213–31
[61] Johnson B K and Prud'homme R K 2003 Flash nanoprecipitation of organic actives and block copolymers using a confined impinging jets mixer *Aust. J. Chem.* **56** 1021–4
[62] Göttert S, Salomatov I, Eder S, Seyfang B C, Sotelo D C, Osma J F and Weiss C K 2022 Continuous nanoprecipitation of polycaprolactone in additively manufactured micromixers *Polymers (Basel)* **14** 1–14
[63] Bally F, Garg D K, Serra C A, Hoarau Y, Anton N, Brochon C, Parida D, Vandamme T and Hadziioannou G 2012 Improved size-tunable preparation of polymeric nanoparticles by microfluidic nanoprecipitation *Polymer* **53** 5045–51
[64] Thandapani G, Prasad S P, Sudha P N and Sukumaran A 2017 Size optimization and *in vitro* biocompatibility studies of chitosan nanoparticles *Int. J. Biol. Macromol.* **104** 1794–806
[65] Sanjeev R, Acharya, Padmanabha R, Acharya S and Niyati A 2015 Optimization of size controlled poly (lactide-co-glycolic acid) nanoparticles using quality by design concept *Asian J. Pharmaceutics* **9** 152–61
[66] Barclay L M 1976 Formation and structure of PVC particles, Die *Angew. Makromol. Chem.* **52** 1–20
[67] Lewis M H and Johnson G R 1981 Agitation scale-up effects during VCM suspension polymerization *J. Vinyl Technol.* **3** 102–6
[68] Biswas A K, Islam M R, Choudhury Z S, Mostafa A and Kadir M F 2014 Nanotechnology based approaches in cancer therapeutics *Adv. Nat. Sci.: Nanosci. Nanotechnol.* **5** 043001
[69] Litzinger D C, Buiting A M J, van Rooijen N and Huang L 1994 Effect of liposome size on the circulation time and intraorgan distribution of amphipathic poly(ethylene glycol)-containing liposomes *Biochim. Biophys. Acta – Biomembranes* **1190** 99–107
[70] Li Y, Stroberg W, Lee T-R, Kim H S, Man H, Ho D, Decuzzi P and Liu W K 2014 Multiscale modeling and uncertainty quantification in nanoparticle-mediated drug/gene delivery *Comput. Mech.* **53** 511–37
[71] Lee T-R, Choi M, Kopacz A M, Yun S-H, Liu W K and Decuzzi P 2013 On the near-wall accumulation of injectable particles in the microcirculation: smaller is not better *Sci. Rep.* **3** 2079
[72] Chen X, Wu Y, Dau V T, Nguyen N T and Ta H T 2023 Polymeric nanomaterial strategies to encapsulate and deliver biological drugs: points to consider between methods *Biomater. Sci.* **11** 1923–47
[73] Salatin S, Barar J, Barzegar-Jalali M, Adibkia K, Kiafar F and Jelvehgari M 2017 Development of a nanoprecipitation method for the entrapment of a very water soluble drug into Eudragit RL nanoparticles *Res. Pharm. Sci.* **12** 1–14
[74] Fessi H, Puisieux F, Devissaguet J P, Ammoury N and Benita S 1989 Nanocapsule formation by interfacial polymer deposition following solvent displacement *Int. J. Pharm.* **55** R1–4
[75] Grabowski N, Hillaireau H, Vergnaud J, Santiago L A, Kerdine-Romer S, Pallardy M, Tsapis N and Fattal E 2013 Toxicity of surface-modified PLGA nanoparticles toward lung alveolar epithelial cells *Int. J. Pharm.* **454** 686–94
[76] Sahoo S K, Panyam J, Prabha S and Labhasetwar V 2002 Residual polyvinyl alcohol associated with poly (D, L-lactide-co-glycolide) nanoparticles affects their physical properties and cellular uptake *J. Control. Release* **82** 105–14
[77] Hoda M, Sufi S A, Cavuturu B and Rajagopalan R 2018 Stabilizers influence drug-polymer interactions and physicochemical properties of disulfiram-loaded poly-lactide-co-glycolide nanoparticles *Future Sci. OA* **4** Fso263
[78] Zakharchenko S, Sperling E and Ionov L 2011 Fully biodegradable self-rolled polymer tubes: a candidate for tissue engineering scaffolds *Biomacromolecules* **12** 2211–5